Supplemental Data

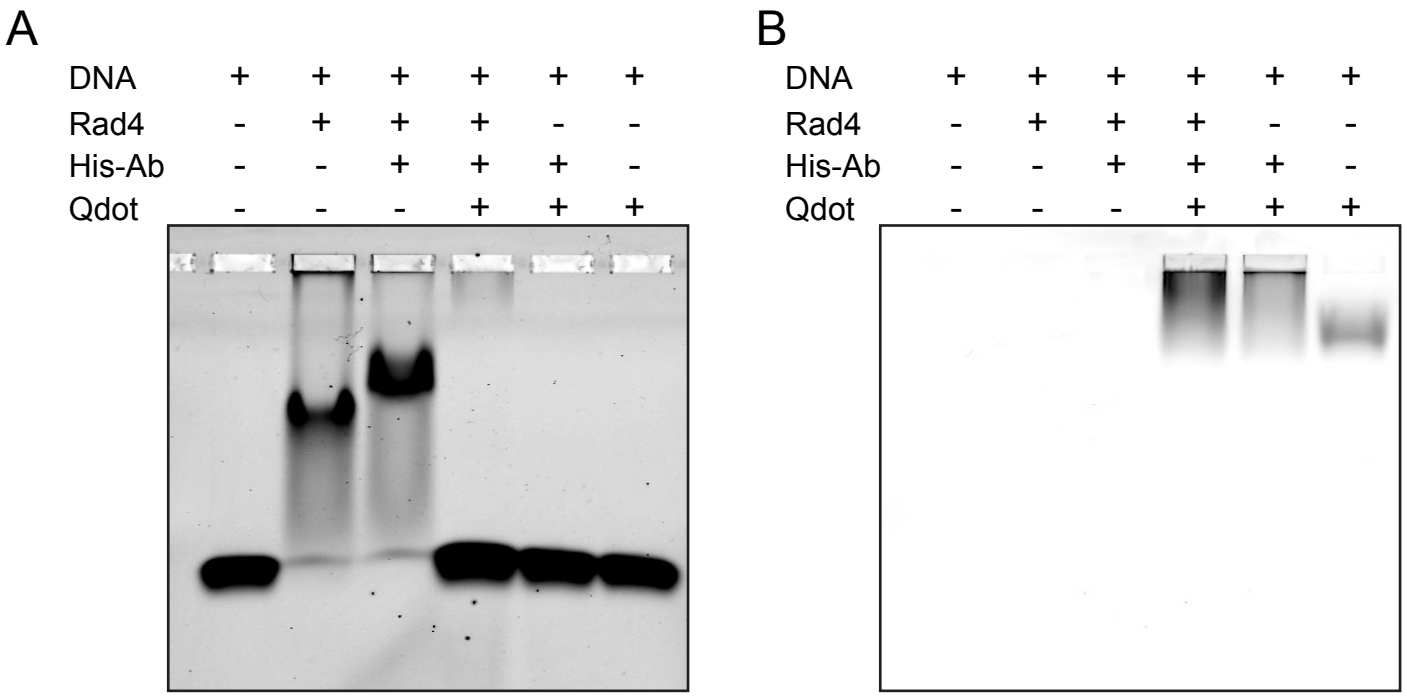

Figure S1. Electrophoretic Mobility Shift Assay of Rad4-Rad23 Conjugated wtih Anti-His Antibody and Quantm Dots, Related to Figure 1

Agarose EMSA gel of Rad4-Rad23 conjugated with anti-His antibody and quantum dots binding to 37bp Fl-dT-containing DNA, imaged using 526 nm (A) and 670 nm (B) emission filters, respectively.

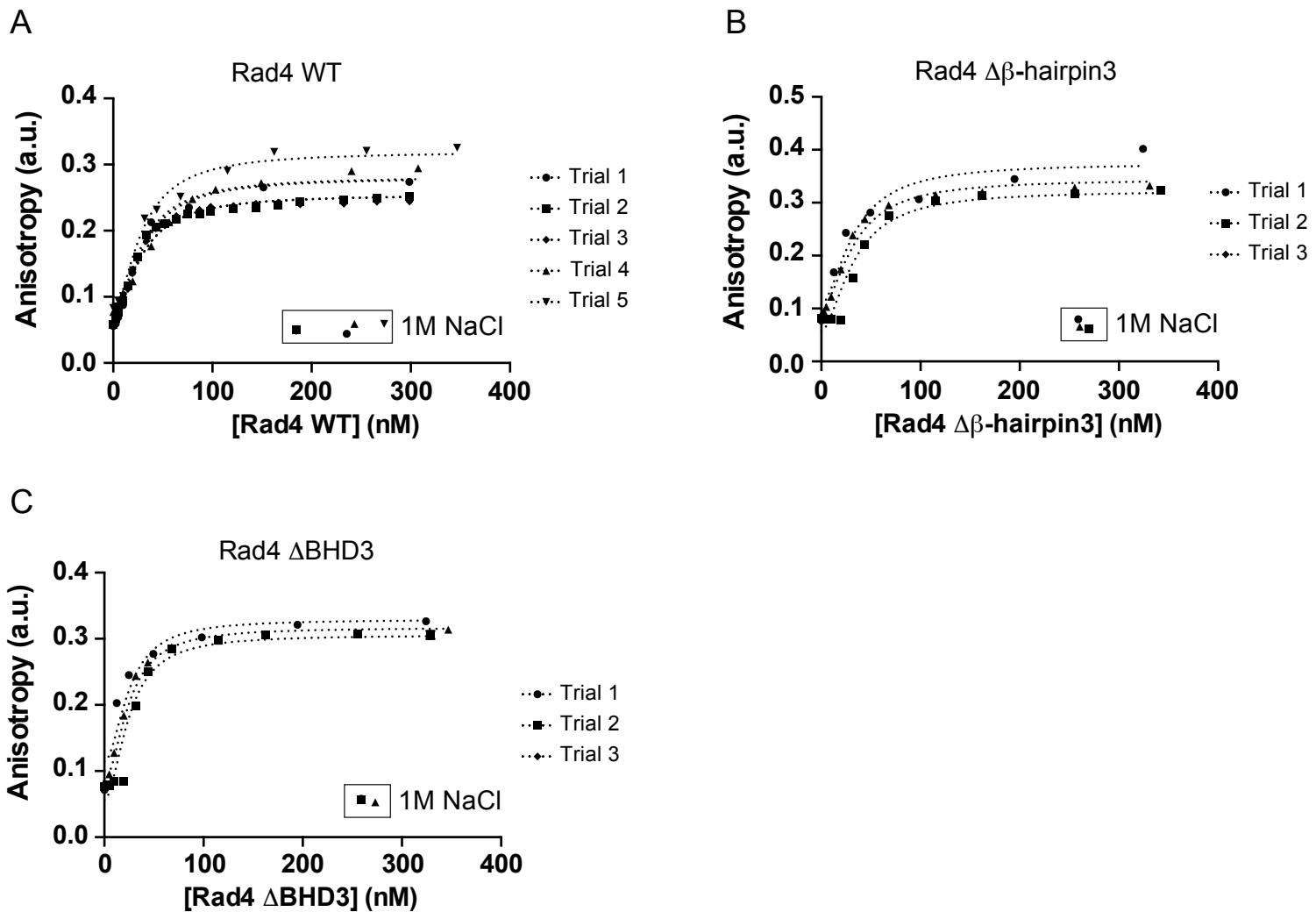

Figure S2. WT and Deletion Mutants of Rad4-Rad23 Bind Stably to Fl-dT Containing Duplex DNA, Measured by Fluorescence Anisotropy, Related to Figure 3

Equilibrium binding experiments of (A) WT, (B) Δβ-hairpin3, and (C) ΔBHD3 were repeated 3-5 times. Dotted curves shown were obtained by fitting replicates from each protein construct globally using a single-site cooperative binding model. Data points in boxes show reversibility of each binding reaction after addition of 1M NaCl.

A

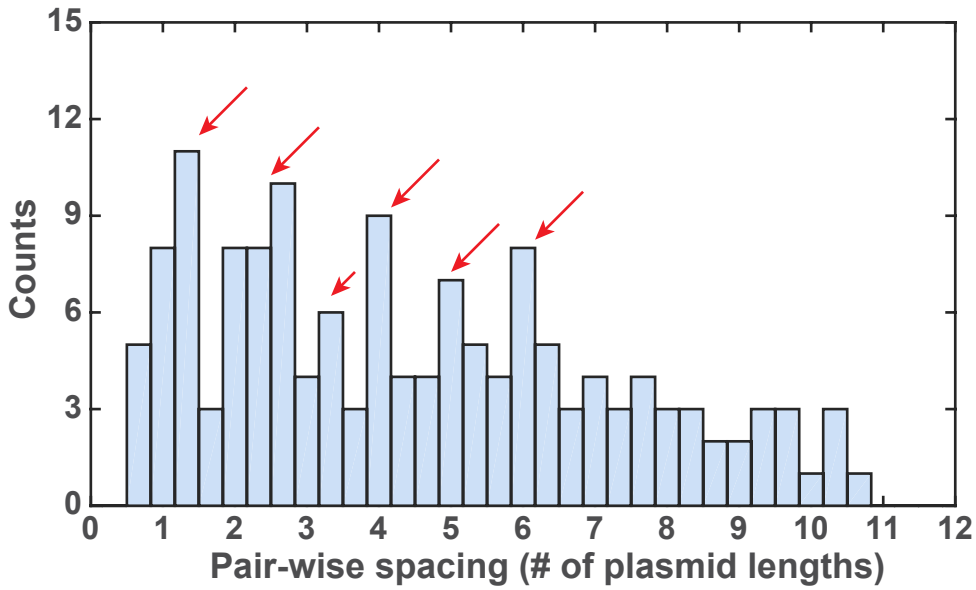

Figure S3. Specific Binding of Rad4-Rad23 on Fl-dT Containing DNA Damage Arrays, Related to Figure 3

(A) Distribution of pair-wise distances between stably bound Rad-Rad23 particles on Fl-dT DNA damage arrays, measured in numbers of plasmid lengths (2030 bp). Red arrows indicate regular integer multiples of up to 6 plasmid lengths.

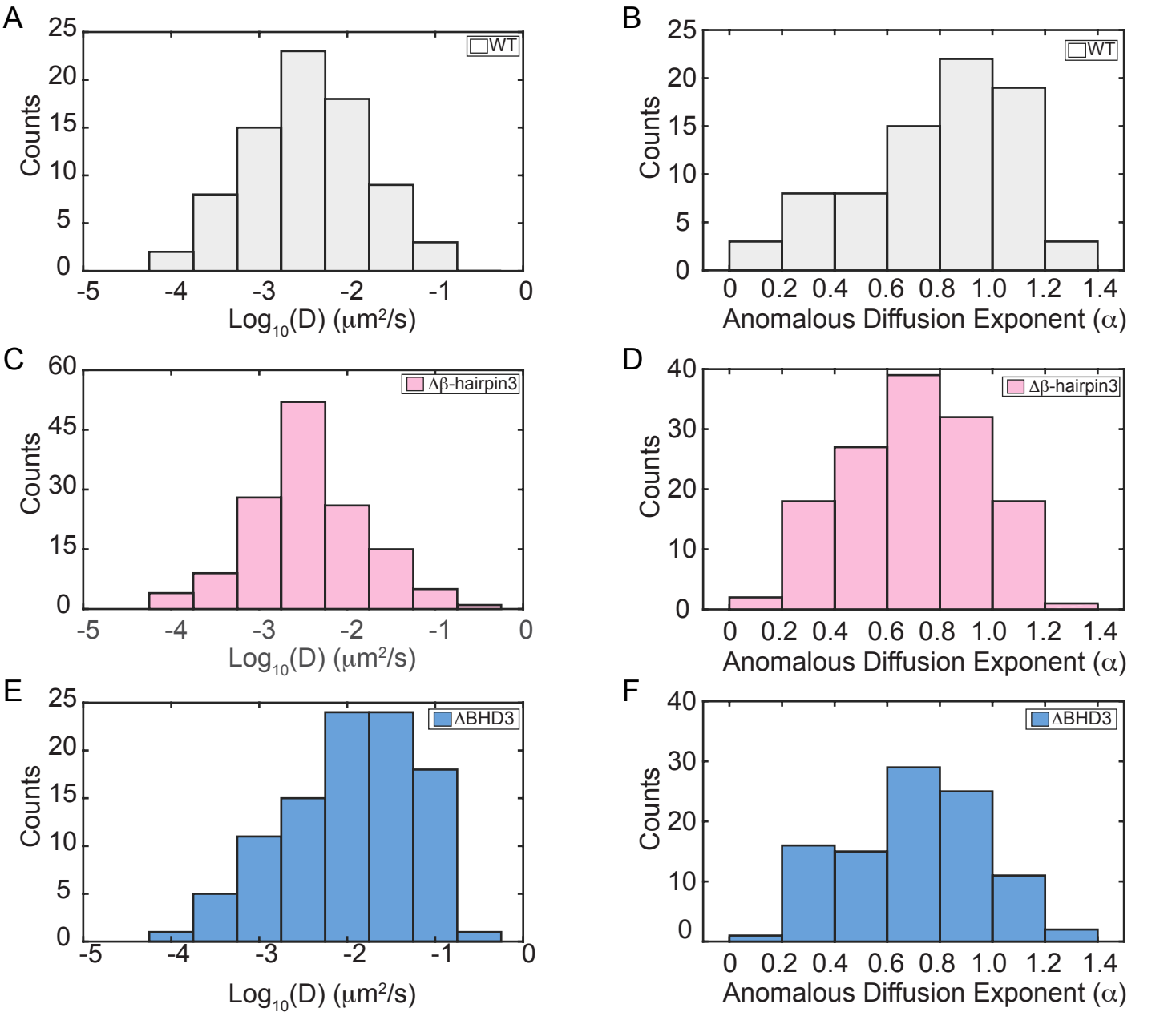

Figure S4. Diffusion behavior of Rad4 WT and Deletion Mutants on UV-irradiated λ-DNA, Related to Figure 4

Distributions of diffusion coefficients $log_{10}D$ and anomalous diffusion exponents α, respectively, of (A) and (B) WT Rad4-Rad23, (C) and (D) Δβ-hairpin3, and (E) and (F) ΔBHD3.

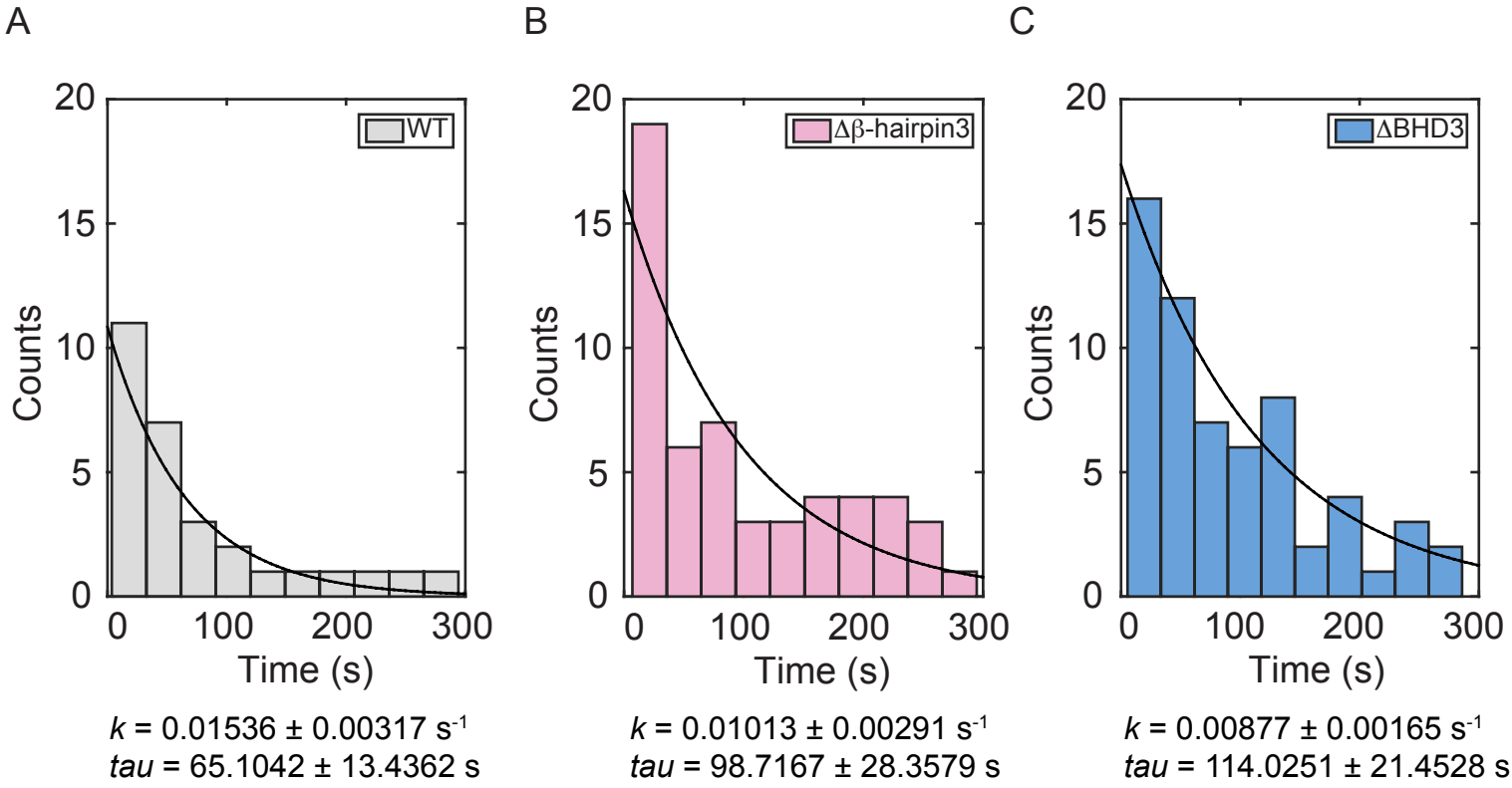

Figure S5. Rad4 WT and Deletion Mutants Share Similar Dissociation Kinetics, Related to Figure 4
(A - C) Single exponential fittings of dwell time histograms of dissociating (A) WT, (B) Δβ-hairpin3, and (C) ΔBHD3 particles.

A

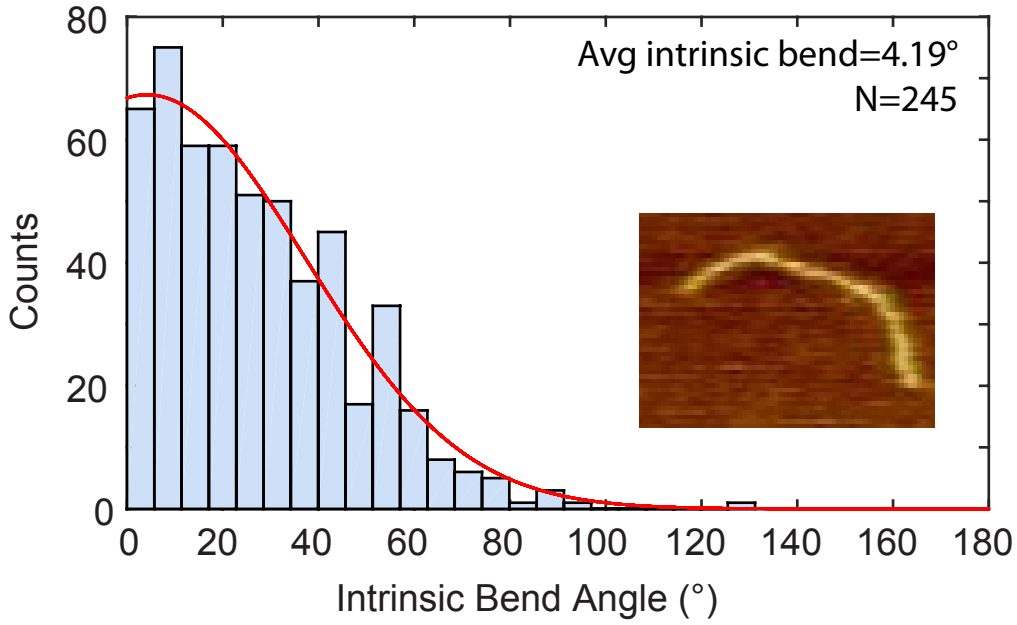

Figure S6. Intrinsic Bend in Fl-dT Containing Duplex DNA, Related to Figure 5
(A) Distribution and Gaussian fitting of intrinsic bend angles of the 538 bp Fl-dT containing DNA fragment used in AFM experiments. Inset: representative AFM image of a 538 bp DNA fragment.

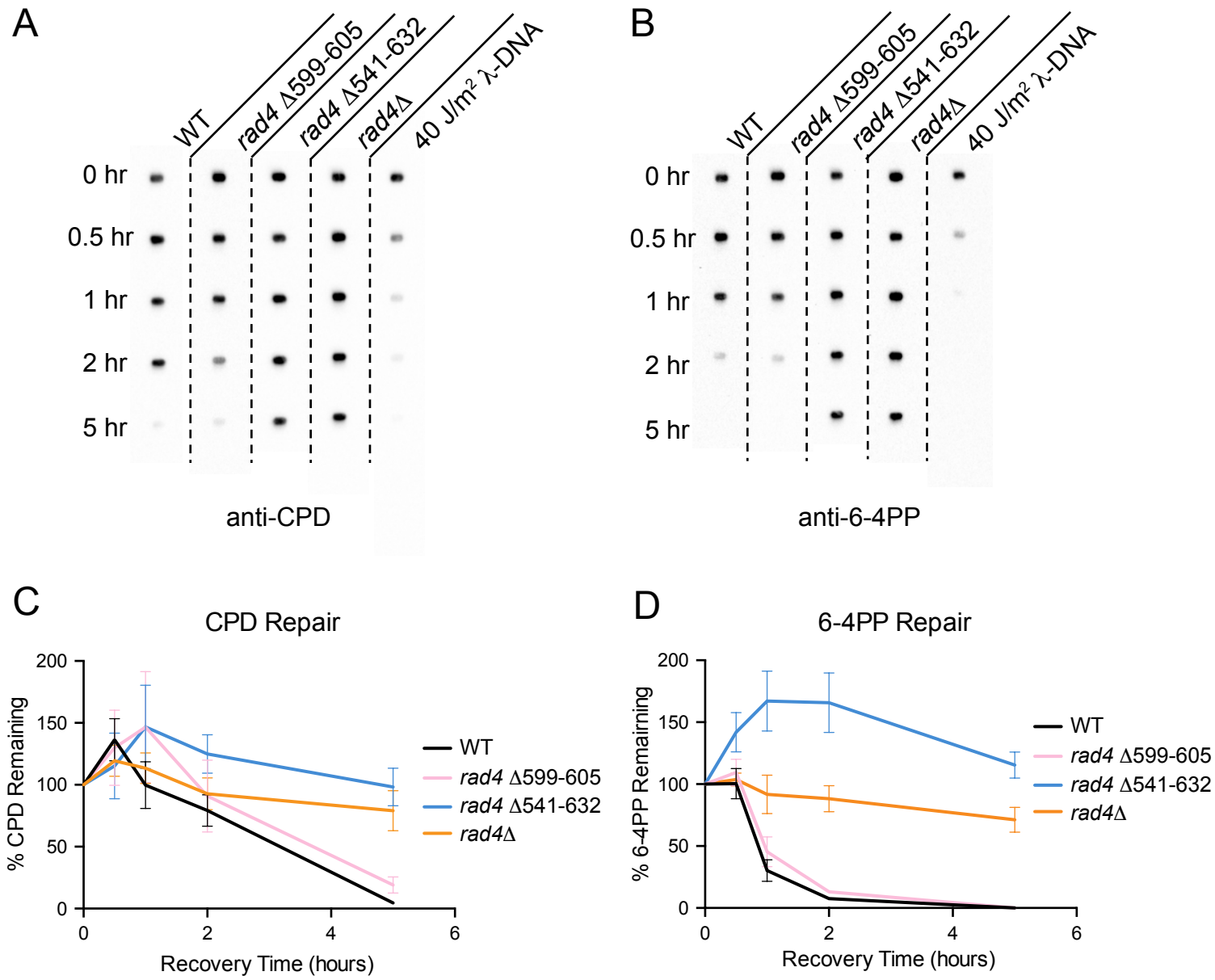

Figure S7. Antibody Slot Blots of CPD and 6-4PP Repair Kinetics, Related to Figure 6
(A) and (B) Representative antibody slot blots against CPD and 6-4PP, respectively.
(C) and (D) Quantitative repair kinetics of CPD and 6-4PP, respectively. Time courses shown are averages of two to three biological repeats, each spotted in triplicates. Error bars represent standard error of the mean of two to three experiments, each done in triplicates.

	WT	Δβ-hairpin3	ΔBHD3
K_D (nM)	28.72 ± 0.65	33.07 ± 1.81	24.89 ± 1.35
Hill coefficient	1.66 ± 0.06	1.72 ± 0.16	1.90 ± 0.18

Table S1. WT and Deletion Mutants of Rad4-Rad23 Bind Tightly to Fl-dT Containing Duplex DNA, Related to Figure 5

Equilibrium dissociation constants (K_D) and Hill coefficients obtained from fitting anisotropy data (3-5 duplicates) with cooperative one-site specific binding model in *Prism 6* (best-fit value ± standard error).

Name	Description	Sequence
OMP007	sgRNA targeting *RAD4*	GATCACAGTTAAGCCAGTTTTAAGGTTTTAGAGCTAG[1]
OMP008	sgRNA targeting *RAD4* (other strand)	CTAGCTCTAAAACCTTAAAACTGGCTTAACTGT
OMP011	Donor DNA for *rad4-Δ599-605* (Forward)	AGGTTTTTGGGGGTGGAATTTGCACCTGCTGTAACTTCTTTTAAGAAG CCAGTTTTAAGTGGCATTGTTGTTGCAAAGTGGCTCAGAGAA
OMP012	Donor DNA for *rad4-Δ599-605* (Reverse)	TTCTCTGAGCCACTTTGCAACAACAATGCCACTTAAAACTGGCTTCTT AAAAGAAGTTACAGCAGGTGCAAATTCCACCCCCAAAAACCT
OMP013	Donor DNA for *rad4-Δ590-615* (Forward)	GAGAATCCTGTGGCAATTAAAGCTGCTAGGTTTTTGGGGGTGGAAAAG TGGCTCAGAGAAGCTATTGAAACCGCTATTGATGGAATAGAG
OMP014	Donor DNA for *rad4-Δ590-615* (Reverse)	CTCTATTCCATCAATAGCGGTTTCAATAGCTTCTCTGAGCCACTTTTC CACCCCCAAAAACCTAGCAGCTTTAATTGCCACAGGATTCTC
OMP015	Donor DNA for *rad4-Δ541-632* (Forward)	GAAGAAGATGAAAGATTATATAGCTTTGAAGACACAGAATTATACCAA GAGGATGATAATAGGAAGGAACATTTGCTTGGTGCTTTGGAG
OMP016	Donor DNA for *rad4-Δ541-632* (Reverse)	CTCCAAAGCACCAAGCAAATGTTCCTTCCTATTATCATCCTCTTGGTA TAATTCTGTGTCTTCAAAGCTATATAATCTTTCATCTTCTTC
OMP017	Donor DNA for *rad4-Δ541-Cterm*[2] (Forward)	GAAGAAGATGAAAGATTATATAGCTTTGAAGACACAGAATTATACAAT GAGGCTGAAACGGTTTGAATAATTAGGAAAGTATGTTTTTAA
OMP018	Donor DNA for *rad4-Δ541-Cterm*[2] (Reverse)	TTAAAAACATACTTTCCTAATTATTCAAACCGTTTCAGCCTCATTGTA TAATTCTGTGTCTTCAAAGCTATATAATCTTTCATCTTCTTC
OMP019	*rad4* screening primer (Forward)	AGGACAGTTGGAAGGCCTAA
OMP020	*rad4* screening primer (Reverse)	GTAGCACTTTCCTCCGCTT
OMP021	*rad4* screening primer (Reverse, for C-term deletion)	ACTCAAGTCCCTGTCCCTCT

Table S2. Oligonucleotides used for constructing *rad4* mutants using CRISPR/Cas9

[1]The 20mer guide sequence is underlined; [2]The *rad4-Δ541-Cterm* mutant contains an additional six amino acids (NEAETV) at the end of the C-terminal deletion.

SUPPLEMENTAL EXPERIMENTAL PROCEDURES

Single-Molecule DNA Tightrope Assay

To visualize protein-DNA interaction in real time, we employed DNA tightrope assay as described elsewhere (Ghodke et al., 2014). Briefly, 5 µm silica beads (Polysicences Inc.) coated with poly-L-lysine (Wako Chemicals) were introduced into a custom flow cell and randomly distributed on coverslip treated with mPEG-succinimidyl valerate MW-5000 (Laysan Bio Inc.). DNA was then introduced at 0.3 ml/min flow rate. N-terminally Histidine-tagged Rad4-Rad23 was conjugated to 655 nm streptavidin Qdots (life technologies) via Penta-His antibody biotin conjugate (Qiagen). The ratio of 1:5:1 for protein:HisAb:Qdot was chosen as previously tested (Ghodke et al., 2014). Typically, the final concentration of labeled Rad4-Rad23 in the flow cell during imaging was ~1.6 nM and proteins were refreshed every two hours. All binding experiments, unless otherwise noted, were carried out in binding buffer containing 5mM BTP-HCl pH 6.8, 75 mM NaCl, 5% glycerol, 0.74 mM CHAPS, 0.5 mg/ml BSA, and 5 mM DTT. Oblique angle fluorescence imaging was performed using a Nikon Eclipse Ti inverted microscope base with a Nikon 100X TIRF objective with 1.45 numerical aperture. Qdots were excited using a 488-nm laser with a power of 1-2 mW at the back focal plane. Qdot emissions were captured on an Andor Neo sCMOS camera using *Nikon Elements Ar* software. Exposure time was either 80 or 100 ms per frame, which resulted in frame rates of 10.92 or 10 fps respectively. Particles were typically recorded for five minutes. The positional accuracy and localization precision of the system have been reported previously to be ~6 nm and ~10 nm, respectively (Ghodke et al., 2014).

Each ND2 file was exported as a time series of TIFF images using Nikon Elements Viewer, imported into ImageJ software (NIH), and saved as a TIFF stack. Kymograph of each protein particle of interest was generated by using the slice function in ImageJ on the image stack, over a line drawn along the trajectory of the particle. Position of the particle is then tracked by fitting the intensity profile of the kymograph at each time point with a one-dimensional Gaussian in ImageJ. Positional data was transferred to Matlab (MathWorks), where given the pixel size (43 nm) and frame rate, a custom-written script calculates the mean squared displacement (*MSD*). To obtain diffusion coefficient *D* and anomalous diffusion exponent α, the *MSD* vs. time step (Δt) curve is fitted to the general model of 1D diffusion(Hughes et al., 2013)

$$MSD = 2D(\Delta t)^{\alpha}$$

The minimum criteria for reporting fitted *D* and α values are such that at least 10% of the entire diffusion trajectory was used in a fitting that produced an R^2 value of 0.8 or higher.

Several criteria have been employed consistently to ensure unbiased classification of particle motion. First, a particle is considered to be motile if its Gaussian-fitted position displacement is greater than three pixels, or ~400 bp at 43 nm/pixel, while motions below three pixels are considered nonmotile. Even though this criterion does act as a constraint in scoring motile particles, as pointed out earlier, the positional accuracy is much higher (~30 bp). As a result, constrained motion may have been conservatively underestimated. To differentiate random versus constrained motion, the criterion arises from the examination of kymographs: random motion covers several thousand base-pairs before reversing direction and usually the total track length of these particles is great distances (10-30 kbp) along the DNA tight rope; whereas constrained motion is seen an oscillatory motion around a central point, the motion in each direction being usually 500-1000 bp.

UV-irradiated λ-DNA and Defined Lesion DNA Damage Arrays

Generation and quantification of UV damage in λ-DNA have been previously described (Ghodke et al., 2014). Briefly, commercially available λ-DNA (New England Biolabs) was diluted in 10 mM Tris-HCl pH 8.5 to 50 ng/μL, deposited in 20 μL aliquots in a sterile petri dish, and exposed to a calibrated UV-C lamp (254 nm) to achieve a total irradiation of 20 or 40 J/m^2 and generate randomly distributed UV-induced photoproducts. A dose-response curve relating lesion frequency to UV dose was generated as previously described through qPCR.

DNA damage arrays containing defined lesions (FI-dT or CPD) were constructed as previously described (Ghodke et al., 2014). Oligonucleotides with custom chemical modifications (Integrated DNA Technologies or TriLink Biotechnologies) were annealed to gapped pSCW01 plasmids (Geng et al., 2011). The annealed products were subsequently first incubated with T4 DNA Ligase (New England Biolabs) to seal the remaining nicks and then linearized with XhoI (New England Biolabs). To obtain DNA substrates of lengths comparable to that of λ-DNA suitable for the tightrope assay, 1 μg linearized plasmids were tandem-ligated with 2 μL T4 DNA Ligase in 20 μL reactions at room temperature for 15 minutes. Due to the

nature of oblique angle illumination in the imaging process, fluorescein molecules incorporated in DNA damage arrays are not visible in tightrope assays.

Atomic Force Microscopy

600 nM Rad4-Rad23 (WT or ΔBHD3) was incubated with 150 nM Fl-dT containing (30% contour length from one end) DNA fragments at room temperature for 30 minutes in AFM binding buffer containing 5mM BTP-HCl pH 6.8, 75 mM NaCl, 5% glycerol, and 0.74 mM CHAPS. Binding reaction was then diluted 50-fold in AFM deposition buffer (25 mM sodium acetate, 10 mM magnesium acetate, and 25 mM HEPES pH 7.5). 10 uL of the dilution was immediately deposited onto freshly cleaved mica surface (SPI Supplies) for 30 seconds, rinsed with 1 mL of filtered water, and dried in a gentle stream of nitrogen. AFM data were collected on a MultiMode V microscope (Bruker Corp.) with an E scanner and Pointprobe® plus noncontact silicon probes (PPP-NCL, Agilent Technologies) in tapping mode. Images (512 × 512 pixels) were captured at a scan rate of ~3 Hz for areas of 1 μm × 1 μm in size using NanoScope 7 software and flattened. For bend angle analysis, AFM images were first exported as TIFF files and then processed with the built-in segmented line and angle tools of ImageJ. Only DNA molecules not crossing itself or others, with both ends clearly visible, and internally-bound protein present were analyzed. Specifically, the contour of each candidate DNA molecule was traced using the segmented line tool in ImageJ. Protein binding positions and total DNA contour lengths were measured in pixels and binding positions were then converted to percentage DNA contour length from the closest end (thus always ≤ 50%). For each internal binding event, the angle tool was used to quantify the degree of DNA bending by manually tracing the paths of DNA immediately next to the sides of protein particles. This measured angle is always the smaller angle of the two and therefore less than or equal to 180°. DNA bend angle was then obtained by subtracting the measured angle from 180° to reflect bending from a straight DNA molecule. Intrinsic DNA bend angles at Fl-dT sites were quantified by first determining positions that are 30% from either end of DNA molecules with the segmented line tool, and then measuring bending with the angle tool at these positions.

Fluorescence Anisotropy

Saturation binding experiments of increasing concentrations of Rad4-Rad23 (WT and variants) to 7.7 nM of 50bp duplex DNA fragment (GAC TAC GTA CTG TTA CGG CTC CAT C**T**C TAC CGC AAT CAG GCC AGA TCT GC, where **T** indicates embedded Fl-dT) were performed on a Cary Eclipse Fluorescence Spectrophotometer (Agilent Technologies) at 37 °C using a set of four matched quartz cuvettes in binding buffer (see above). Embedded fluorescein was excited at 485 nm and its emission collected at 520 nm, with slit widths of 5 and 10 nm for excitation and emission, respectively. In each experiment, G-factor was determined once at the beginning. At each titration point, protein was added and the cuvette tapped for mixing. After 3 minutes of incubation, anisotropy measurement was made in triplicates. Final reading was reported as mean ± standard deviation. At the end of each experiment, 5M NaCl was added to cuvette to reach 1M NaCl final concentration. All binding events were shown to be reversible as anisotropy returned to initial values upon the addition of 1 M NaCl. In order to obtain equilibrium dissociation constants (K_d), binding isotherms (anisotropy vs. protein concentration) were fitted to the following single-site cooperative binding model using *Prism 6* (GraphPad Software):

$$r = a \cdot \frac{x^n}{{K_d}^n + x^n} + b$$

where *r* is anisotropy, *a* is maximum anisotropy at saturation, *x* is protein concentration, *n* is the Hill coefficient, K_d is the equilibrium dissociation constant, and *b* is the initial anisotropy without protein (Pagano et al., 2011). Parameters *n* and K_d were shared across repeats of the same protein variant for global fitting.

Agarose Gel EMSA

1 uM Rad4-Rad23 was incubated with equal amount of 1 uM biotinylated His-antibody (QIAGEN) at 4 ºC for 1 hour. 500 nM Rad4-Ab complex was then incubated with equal amount of 1 uM 705 nm streptavidin-coated quantum dots (life technologies) at 4 ºC for 1 hour. Binding reactions were carried out in 10 uL volumes at room temperature for 30 minutes with 10 nM 37 bp dsDNA (CCG AGT CAT TCC **T**GC AGC GAG TCC ATG GGA GTC AAA T, where **T** indicates embedded Fl-dT) and one of the following: 200 nM Rad4, 200 nM Rad4-Ab, 167 nM Rad4-Ab-Qdot, 200 nM Ab-Qdot, or 200 nM Qdot. A 1% agarose gel was cast in ½X TBE and pre-run on ice at 80V for 30 minutes before samples were loaded and run on ice at 80V for 60 minutes. Gel image was scanned using a Typhoon 9400 Variable Mode Imager (GE Healthcare Life Sciences) set to fluorescent mode with excitation wavelength 488 nm, emission wavelengths 526 nm

and 670 nm for fluorescein and Qdot signals, respectively. The fact that Rad4-Ab-Qdot conjugates on DNA were observed by fluorescence microscopy suggests that EMSA is greatly underestimating the DNA binding capacity of these conjugates.

Estimation of Hydrodynamic Radii

Radius of gyration ($R_{g,Rad4} = 3.03\ nm$) of WT Rad4-Rad23 is estimated by `WinHYDROPRO` (Ortega et al., 2011). Crystal structure of the protein complex (`2QSF`) is imported into the software and the following constants are used for estimation with the 'shell-model from atomic level' option: molecular weight $MW = 96.94\ kDa$, room temperature $\mathrm{T} = 298\ \mathrm{K}$, viscosity of water $\eta = 0.89 \times 10^{-3}\ \mathrm{Pa \cdot s}$ at room temperature ($298\ \mathrm{K}$). Hydrodynamic radius (R_H) is then estimated through the relationship:

$$R_{H,Rad4} = \frac{R_{g,Rad4}}{\rho} = 3.91\ nm$$

where $\rho = (\frac{3}{5})^{1/2}$ for spherical molecules (Burchard et al., 1980).

An effective hydrodynamic radius of the quantum dot-labeled Rad4-Rad23 complex is estimated based on the combined hydrodynamic volume of a quantum dot (QD) and Rad4-Rad23 such that:

$$R_{H,eff} = ({R_{H,QD655}}^3 + {R_{H,Rad4}}^3)^{1/3} = 11.65\ nm$$

where $R_{H,QD655} = 11.5\ nm$ is the hydrodynamic radius of a 655 nm SAQD (Arnspang et al., 2012).

Estimation of Theoretical Limit of Diffusion Coefficient

The diffusion coefficient *D* for a sphere diffusing in fluid can be calculated using the Stokes-Einstein equation:

$$D = \frac{k_B T}{\xi}$$

where ξ is the friction term, k_B is the Boltzmann constant and *T* is temperature. At room temperature ($\mathrm{T} = 298\ \mathrm{K}$), $k_B T = 4.11 \times 10^{-21} J$. For a globular protein of radius *R* diffusing linearly on DNA while tracking the helix in solution with viscosity η, the friction term ξ has been derived (Bagchi et al., 2008):

$$\xi = 6\pi\eta R + \left(\frac{2\pi}{10.5\ BP}\right)^2 [8\pi\eta R^3 + 6\pi\eta R_{OC}(R)^2]$$

where $1\ BP = 0.34\ nm$ and R_{OC} is the off-center distance from the center of mass of the protein to the helical axis of DNA. Using the effective hydrodynamic radius $R_{H,eff} = R$ as calculated above, under the idealization that the sphere is offset from the DNA helical axis by the radius of DNA ($r_{DNA} = 1\ nm$) such that $R_{OC} = R_{H,eff} + r_{DNA} = 12.65\ nm$, we obtain the theoretical limit to diffusion for the QD-Rad4 complex:

$$D_{lim} = \frac{k_B T}{6\pi\eta R + \left(\frac{2\pi}{10.5\ BP}\right)^2 [8\pi\eta R^3 + 6\pi\eta R_{OC}(R)^2]} = 0.0199\ \mu m^2/s$$

Calculation of Energy Barrier to Free Diffusion

The energy barrier to free diffusion can be calculated by using the measured and theoretical diffusion coefficients *D* and the Arrhenius relation (Blainey et al., 2006; Kad et al., 2010):

$$k = e^{-E/k_B T}$$

where *k* is the stepping rate in units of *steps/s* and related to D such that

$$k = 2D/l^2$$

where *l* is the step size, assumed to be a single base pair. Therefore, the barrier to free diffusion is:

$$\Delta E = \ln\left(\frac{k_{lim}}{k_{expt}}\right) = \ln\left(\frac{D_{lim}}{D_{expt}}\right) \cdot k_B T$$

where D_{lim} is the theoretical limit to diffusion coefficient as calculated above, and D_{expt} is the experimental measurement. Using the equation above and experimental values for diffusion coefficients of constrained and random Rad4-Rad23 WT on UV irradiated λ-DNA, $0.0040 \pm 0.0013\ \mu m^2/s$ and $0.0138 \pm 0.0033\ \mu m^2/s$ respectively, we calculate that energy barriers to free diffusion for constrained and random movers are

$$\Delta E_{cons} = 1.60 \pm 0.32\ k_B T$$

$$\Delta E_{rand} = 0.37 \pm 0.24\ k_B T$$

Estimation of Residence Time at Each Base Pair

The dwell time (τ_{bp}) of Rad4-Rad23 at each base pair during linear diffusion is estimated as the inverse of the stepping rate

$$\tau_{bp} = \frac{1}{k} = \frac{1}{2D/l^2} = l^2/2D$$

For constrained motion, $\tau_{bp} \cong 15\ \mu s$. For random diffusion, $\tau_{bp} \cong 4\ \mu s$. This microsecond time scale of Rad4 residence time per site is largely consistent with that of various other proteins undergoing one-dimensional diffusion on DNA and indeed much slower than the expected undamaged DNA opening times of Rad4, estimated to be much longer than 5-10 ms (Chen et al., 2015).

Estimation of Minimum Target Site Energy

Given the genome size M, the minimum energy requirement at target site (E_0) for efficient recognition is given by (Slutsky and Mirny, 2004)

$$E_0 = \sqrt{2 \ln M}\ k_B T$$

For yeast genome $M = 1.21{\times}10^7 bp$ (Goffeau et al., 1996), $E_0 = 5.71\ k_B T$.

Estimation of Genome Search Time

Diffusion coefficients of unlabeled Rad4-Rad23 can be predicted using the Arrhenius equation and the energy barrier calculations from above (Hughes et al., 2013). Specifically:

$$D_{Rad4,cons} = D_{lim} \cdot e^{-\frac{\Delta E_{cons}}{k_B T}} = 0.091 \pm 0.030\ \mu m^2/s$$

$$D_{Rad4,rand} = D_{lim} \cdot e^{-\frac{\Delta E_{rand}}{k_B T}} = 0.312 \pm 0.076\ \mu m^2/s$$

Whereas the search range ($\mathcal{R}$) for each encounter of Rad4 with DNA can also be estimated as $\mathcal{R} = \sqrt{\frac{16Dt}{\pi l^2}}$ where l is a single base pair and *t* is the time of encounter(Hughes, 1995), or lifetime of Rad4-Rad23 on DNA (Figure S5).

$$\mathcal{R}_{Rad4,cons} = (5.5 \pm 1.0){\times}10^3 bp$$

$$\mathcal{R}_{Rad4,rand} = (2.79 \pm 0.45){\times}10^4 bp$$

Knowing the yeast genome size and that there are ~870 copies of Rad4 per cell (Ghaemmaghami et al., 2003), we can calculate the least number of encounters required such that the total diffusion range covers the entire genome (Hughes et al., 2013). Assuming distribution of motion types similar to that observed from WT protein on UV irradiated λ-DNA:

$$\#\ encounters = \frac{1.2{\times}10^7 bp}{\#\ Rad4\ \cdot \left(\%constrained\ {\times}\mathcal{R}_{Rad4,cons} + \%random{\times}\mathcal{R}_{Rad4,rand}\right)} = 2.22 \pm 0.29$$

Therefore, the fastest possible time needed to search the entire genome of yeast is

$$time\ required = \#\ encounters \times \frac{time}{encounter} = 145 \pm 35\ sec$$

or roughly two to three minutes.

RAD4 Mutant Strain Construction, UV Survival Measurements, and Western Blotting

RAD4 deletion mutants were generated in yeast using the CRISPR-Cas9 system, as described previously (Laughery et al., 2015). Briefly, wild-type yeast strains (*RAD4* or *RAD4-3xFLAG*) were transformed with two plasmids, pT022 and pT040-RAD4, to generate double strand breaks at the *RAD4* gene that were repaired using oligonucleotide templates containing the desired Rad4 deletions (e.g., *rad4 Δ599-605*). pT022 expresses the Cas9 endonuclease and contains the *LEU2* selection marker. pT040-RAD4 harbors the *URA3* selection marker and expresses a single guide-RNA (sgRNA) that targeted the Cas9 endonuclease to the yeast *RAD4* gene to generate a DNA double strand break. By providing donor DNA (double stranded oligonucleotides, see Table S2) containing Rad4 deletions, the targeted *rad4* mutations were introduced into the chromosomal *RAD4* locus by homologous recombination. *RAD4* deletion mutants were confirmed by PCR amplification of isolated genomic DNA and verified by DNA sequencing. The pT022 and pT040-RAD4 plasmids were removed from the *rad4* mutant strains by screening on plates lacking Leucine and 5-Fluoroorotic acid (FOA) counter selection.

To measure UV sensitivity, yeast cells were grown to mid-log phase in YPD (OD_{600} ≈ 0.8). Each culture was serially diluted, spotted on YPD plates, and irradiated with UV light (254 nm) at the indicated UV doses. Plates were immediately wrapped with aluminum foil after UV treatment and incubated at 30˚C for ~72 hr. For the quantitative UV survival assay, yeast cells were spread on YPD plates and then irradiated with UV light at the indicated doses. Plates were incubated in the dark at 30˚C prior to colony counting to determine the percentage of viable colonies.

To assess Rad4 protein level in each yeast strain, yeast whole cell extracts were prepared from 5 ml of yeast culture. Cells are incubated in 0.1 M NaOH for 5 min at room temperature, followed by boiling cells in 100 µl of 1· SDS-PAGE sample buffer for 7 min. After centrifugation, different volumes (3, 6, and 9 µl) of the supernatant for each strain were loaded in an 8% SDS gel. The presence of FLAG-tagged Rad4

protein was detected using anti-FLAG antibody (M2, Sigma). Tubulin was also probed with anti-tubulin antibody (Santa Cruz Biotech) as the loading control.

CPD Repair Kinetics by T4 Endo V Digestion

Exponentially growing yeast cells carrying WT and mutant Rad4 constructs were irradiated with 50 J/m^2 UVC and then repaired for 60 or 120 minutes. Genomic DNA was isolated and digested with CPD-specific T4 endo V to generate single strand breaks at CPD sites. DNA was then separated on a 1.2% alkaline agarose gel and fragmented DNA was detected with SYBR Gold (Bespalov et al., 2001). DNA signal was scanned with a Typhoon FLA 7000 laser scanner (GE Healthcare Life Sciences), and repair was analyzed using ImageQuant software (GE Healthcare Life Sciences). Under these experimental conditions, 50 J/m^2 produced 1 CPD per 4 kbp.

CPD and 6-4PP Repair Kinetics by Antibody Slot Blots

Exponentially growing yeast cells (OD600 ~ 0.8) carrying WT and mutant Rad4 constructs were collected and re-suspended in 1X PBS before irradiated with 100 J/m^2 UVC, collected, and then allowed to recover in YPD in the dark for up to five hours. Genomic DNA from 10 mL cell culture aliquots taken at various time points was extracted with YeaStar Genomic DNA kit (Zymo Research) and quantified with PicoGreen (Invitrogen) on a NanoDrop 3300 fluorospectrometer (Thermo Scientific). Antibody slot blot assays were performed as previously described (Parikh et al., 2015). Briefly, equal amounts of DNA were spotted in triplicates on Amersham Hybond-N+ membrane (GE Healthcare Life Sciences) with Minifold 1 Spot-Blot System (GE Healthcare Life Sciences). DNA was baked on membrane at 80ºC for 2.5 hours and blocked at room temperature in 1X TBS containing 0.3% Tween20 (TBS-T) and 5% non-fat dry milk for one hour. UV lesions were probed by incubating membrane overnight with primary antibodies against CPD (Kamiya Biomedical) or 6-4PP (Cosmo Bio) in 1X TBS-T at 4ºC. Blots were washed in 1X TBS-T, incubated with HRP-conjugated anti-mouse secondary antibody for 1 hour at room temperature when appropriate, developed with SuperSignal West Femto Maximum Sensitivity Substrate (Thermo Scientific), then imaged on ChemiDoc MP (Bio-Rad), and quantified using Image Lab Software (Bio-Rad). Under these experimental conditions, 100 J/m^2 produced ~2.6 CPD and ~1 6-4PP per 2 kbp.

Estimation of Rate of Photoproduct Removal

Rates of photoproduct removal by WT Rad4-Rad23 can be calculated from estimated lesion frequency (1 CPD/4 kbp under 50 J/m^2 in T4 Endo V digestion assays, ~2.6 CPD and ~1 6-4PP per 2 kbp under 100 J/m^2 in antibody slot blot assays) based on the copy number of Rad4-Rad23 (~870/cell) (Ghaemmaghami et al., 2003) and $T_{1/2}$ (times to accomplish 50% repair).

$$Rate\ of\ Photoproduct\ Removal = \frac{Lesion\ Frequency \times yeast\ genome\ size}{2 \times Rad4\ copy\ numer \times T_{1/2}}$$

From T4 Endo V digestion assays

$$Rate\ of\ CPD\ Removal \sim 1.6\ CPDs/Rad4/hour$$

From antibody slot blot assays:

$$Rate\ of\ CPD\ Removal \sim 3\ CPDs/Rad4/hour$$

$$Rate\ of\ 64PP\ Removal \sim 3.6\ 64PPs/Rad4/hour$$

SUPPLEMENTAL REFERENCES

Arnspang, E.C., Brewer, J.R., and Lagerholm, B.C. (2012). Multi-color single particle tracking with quantum dots. PloS one *7*, e48521.

Bagchi, B., Blainey, P.C., and Xie, X.S. (2008). Diffusion constant of a nonspecifically bound protein undergoing curvilinear motion along DNA. The journal of physical chemistry. B *112*, 6282-6284.

Bespalov, V.A., Conconi, A., Zhang, X., Fahy, D., and Smerdon, M.J. (2001). Improved method for measuring the ensemble average of strand breaks in genomic DNA. Environ Mol Mutagen *38*, 166-174.

Blainey, P.C., van Oijen, A.M., Banerjee, A., Verdine, G.L., and Xie, X.S. (2006). A base-excision DNA-repair protein finds intrahelical lesion bases by fast sliding in contact with DNA. Proceedings of the National Academy of Sciences of the United States of America *103*, 5752-5757.

Burchard, W., Schmidt, M., and Stockmayer, W.H. (1980). Information on Polydispersity and Branching from Combined Quasi-Elastic and Intergrated Scattering. Macromolecules *13*, 1265-1272.

Chen, X., Velmurugu, Y., Zheng, G., Park, B., Shim, Y., Kim, Y., Liu, L., Van Houten, B., He, C., Ansari, A.*, et al.* (2015). Kinetic gating mechanism of DNA damage recognition by Rad4/XPC. Nature communications *6*, 5849.

Geng, H., Du, C., Chen, S., Salerno, V., Manfredi, C., and Hsieh, P. (2011). In vitro studies of DNA mismatch repair proteins. Analytical biochemistry *413*, 179-184.

Ghaemmaghami, S., Huh, W.K., Bower, K., Howson, R.W., Belle, A., Dephoure, N., O'Shea, E.K., and Weissman, J.S. (2003). Global analysis of protein expression in yeast. Nature *425*, 737-741.

Ghodke, H., Wang, H., Hsieh, C.L., Woldemeskel, S., Watkins, S.C., Rapic-Otrin, V., and Van Houten, B. (2014). Single-molecule analysis reveals human UV-damaged DNA-binding protein (UV-DDB) dimerizes on DNA via multiple kinetic intermediates. Proceedings of the National Academy of Sciences of the United States of America *111*, E1862-1871.

Goffeau, A., Barrell, B.G., Bussey, H., Davis, R.W., Dujon, B., Feldmann, H., Galibert, F., Hoheisel, J.D., Jacq, C., Johnston, M.*, et al.* (1996). Life with 6000 genes. Science *274*, 546, 563-547.

Hughes, B.D. (1995). Random walks and random environments (Oxford; New York: Clarendon Press; Oxford University Press).

Hughes, C.D., Wang, H., Ghodke, H., Simons, M., Towheed, A., Peng, Y., Van Houten, B., and Kad, N.M. (2013). Real-time single-molecule imaging reveals a direct interaction between UvrC and UvrB on DNA tightropes. Nucleic acids research *41*, 4901-4912.

Kad, N.M., Wang, H., Kennedy, G.G., Warshaw, D.M., and Van Houten, B. (2010). Collaborative dynamic DNA scanning by nucleotide excision repair proteins investigated by single- molecule imaging of quantum-dot-labeled proteins. Molecular cell *37*, 702-713.

Laughery, M.F., Hunter, T., Brown, A., Hoopes, J., Ostbye, T., Shumaker, T., and Wyrick, J.J. (2015). New vectors for simple and streamlined CRISPR-Cas9 genome editing in Saccharomyces cerevisiae. Yeast.

Ortega, A., Amoros, D., and Garcia de la Torre, J. (2011). Prediction of hydrodynamic and other solution properties of rigid proteins from atomic- and residue-level models. Biophysical journal *101*, 892-898.

Pagano, J.M., Clingman, C.C., and Ryder, S.P. (2011). Quantitative approaches to monitor protein-nucleic acid interactions using fluorescent probes. RNA *17*, 14-20.

Parikh, D., Fouquerel, E., Murphy, C.T., Wang, H., and Opresko, P.L. (2015). Telomeres are partly shielded from ultraviolet-induced damage and proficient for nucleotide excision repair of photoproducts. Nature communications *6*, 8214.

Slutsky, M., and Mirny, L.A. (2004). Kinetics of protein-DNA interaction: facilitated target location in sequence-dependent potential. Biophysical journal *87*, 4021-4035.